I&EC research
Industrial & Engineering Chemistry Research

Article

Cite This: Ind. Eng. Chem. Res. 2019, 58, 8743−8749

pubs.acs.org/IECR

Applications of 3D Potassium-Ion Pre-Intercalated Graphene for Perovskite and Dye-Sensitized Solar Cells

Wei Wei, Meijia Li, and Yun Hang Hu*

Department of Materials Science and Engineering, Michigan Technological University, 1400 Townsend Drive, Houghton, Michigan 49931-1295, United States

Supporting Information

ABSTRACT: 3D potassium-ion preintercalated graphene (KIPIG), which was recently invented via the reaction of potassium and CO, shows unique properties including large accessible surface area and excellent electrical conductivity for electrodes. Herein, it was revealed that the perovskite solar cells (PSC) and dye-sensitized solar cells (DSSC) with KIPIG electrode exhibited high power conversion efficiencies of 7.81% and 9.12%, respectively. This work not only proves that 3D KIPIG is an efficient electrode material, but also provides a strategy to reduce the fabrication cost of solar cells.

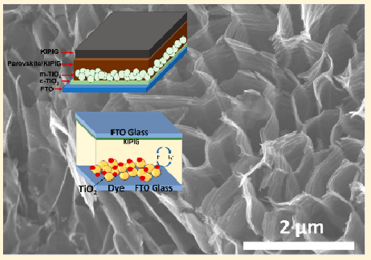

1. INTRODUCTION

Over the past few years, the increasing demand for energy and the cyclic nature of renewable energy sources has stimulated rapid development of methods for sustainable energy conversion and storage technologies.[1] One efficient way to convert the largest single available source of renewable energy—solar energy—into electricity is using solar cells. The dye-sensitized solar cells (DSSCs) and perovskite solar cells (PSCs) are considered to be the most promising devices for the next-generation of solar cells.[2] As one of three main components in a typical DSSC,[3] the counter electrode must have good electrical conductivity and superior electrocatalytic activity.[3−8] Platinum meets the requirements as a standard counter electrode,[9] but its application is limited by its high price and scarcity. Thus, development of efficient and inexpensive counter electrode materials is necessary to replace platinum.[10,11] Conducting polymers,[7] metal sulfides,[12] metal carbides,[13] metal nitrides,[6] and metal oxides[4,14] have been reported as highly efficient DSSC counter electrodes. Moreover, to reduce the cost and enhance the stability, carbon nanotubes and graphene have been explored to replace Pt.[15−18] Furthermore, 3D porous texture of carbon materials, which provides a lower resistance and shorter diffusion pathways, is strongly recommended for the fabrication of DSSCs.

On the other hand, the emergence of methylammonium lead halides in 2009 attracted great interest into lead-halide perovskites as efficient, inexpensive solar absorbers.[19−21] Perovskite solar cells (PSCs) have showed great potential for thin-film low cost photovoltaic technology.[19,22] However, there are some issues that need to be addressed before the commercialization of perovskite solar cells, such as high cost because of employment of costly materials (spiro-OMeTAD as hole transport material (HTM) and gold or silver as electrode). Therefore, it is desired to employ earth abundant and cheap materials to reduce the cost of the perovskite solar cells.[23] Etgar et al. reported the first HTM free perovskite solar cells with efficiency of 5%.[24] This proved that the perovskite could act as not only a hole transport material, but also a light absorber. Moreover, the manufacturing process of the PSC device can be simplified, its cost reduced, and its stability improved by eliminating the HTM layer. Furthermore, the future application of the device is also limited by expensive Au-based back contact. For this reason, inexpensive carbon nanomaterials,[17,25−31] such as carbon nanotubes[32−34] and graphene,[35,36] were introduced into the HTM-free PSCs.

Numerous efforts have been devoted to produce tailored porous carbon materials and activated mesoporous carbon. However, the electrical conductivity of carbon materials will decrease sharply due to its porous structure. It is still a challenge to synthesize a material with both high electrical conductivity and specific surface area. It is demonstrated that the conductivity of carbon materials can be increased by doping alkali metals.[37−41] However, the dopants can be easily oxidized because they are located on the surface. This issue can be solved if the alkali-metal could be protected by carbon atoms. Such hypothetical materials have been successfully synthesized in our previous study, in which the highly conductive porous Na-embedded carbon nanowalls with large surface areas were successfully synthesized.[42] Furthermore, the Na embedded carbon nanowalls exhibited excellent performance for perovskite solar cells[43] and supercapacitors.[44] Very recently, we moved forward to explore the feasibility of synthesizing a new type of 3D potassium-ion preintercalated graphene (KIPIG) by a simple reaction between K and CO. Furthermore, this potassium-ion preintercalated graphene exhibited excellent performance as electrodes for aqueous

Received: February 9, 2019
Revised: April 19, 2019
Accepted: May 7, 2019
Published: May 7, 2019

DOI: 10.1021/acs.iecr.9b00795
Ind. Eng. Chem. Res. 2019, 58, 8743−8749

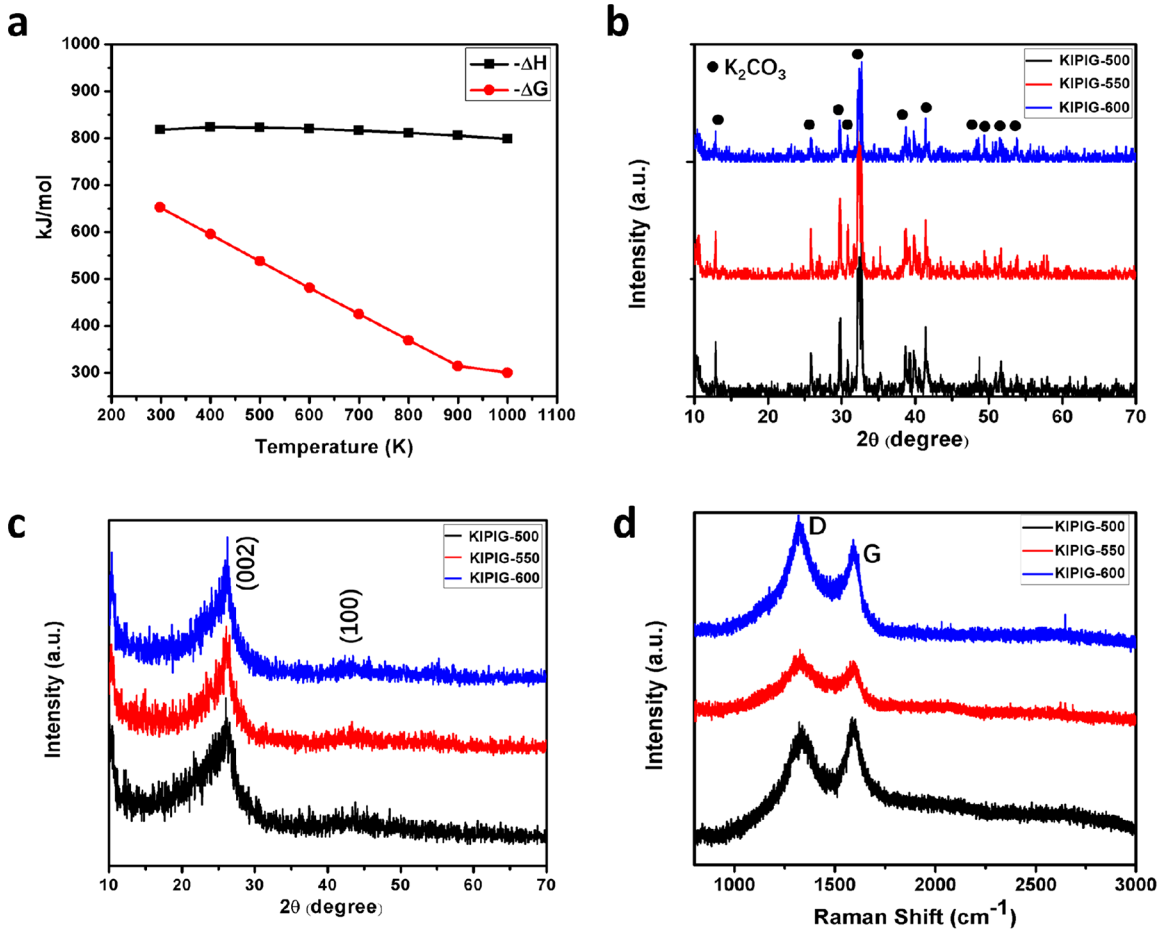

Figure 1. (a) Thermodynamic calculation results of the reaction. (b) XRD patterns of solid products from the reaction between K and CO. (c) XRD patterns of solid products from the reaction between K and CO after HCl treatment. (d) Raman spectra of solid products from the reaction between K and CO after HCl treatment.

symmetrical supercapacitors.[45] In this work, this novel material was systematically explored for DSSCs and PSCs, which revealed its excellent performance of 9.12% and 7.81% for DSSCs and PSCs, respectively.

2. EXPERIMENTAL SECTION

2.1. Synthesis and Characterization of Carbon Nanomaterials. 3D potassium-ion preintercalated graphene (KIPIG) was synthesized with our method, which was reported in our previous paper.[45] Potassium (K) (Aldrich) was used to react with CO in a ceramic tube for 12 h at a selected temperature of 500, 550, or 600 °C. The solid products were treated by 36.5 wt % hydrochloric acid and deionized water washing, respectively. The black KIPIG power was obtained after centrifugation separation and dried in the oven. The KIPIG samples were characterized by a Scintag XDS-2000 powder diffract meter with Cu Kα (λ = 1.5406 Å) radiation for X-ray diffraction (XRD) patterns, Hitachi-4700 field emission scanning electron microscope (FESEM) with energy dispersive spectroscopy (EDS) and JEOL JEM-2010F transmission electron microscope (TEM) for SEM and TEM images, Olympus BX41 spectrometer with a helium−neon laser to excite the samples for Raman spectra, Element analyzer (Control Equipment Corporation model 240XA) for element compositions, Physical adsorption instrument (Micromeritics ASAP 2000) for measurement of surface area and pore size distribution. Sheet resistance of carbon nanomaterial film was measured by Jandel four-point system with RM3 test unit. The carbon nanomaterial films were prepared by doctor-blading method. The inductively coupled plasma (ICP) optical emission spectrometry (OES) was conducted at PerkinElmer Optima 7000 DV ICP-OES.

2.2. Preparation and Characterization of DSSCs. *2.2.1. Preparation and Characterization of Counter Electrodes.* A homogeneous paste was prepared by mixing the KIPIG powder with alcohol. The counter electrode was fabricated by doctor-blading the paste onto a clean Fluorine-doped Tin Oxide (FTO) glass plate, followed by heat treatment at 80 °C for 4 h. A model 6000 micromanipulator was used to measure the thickness (about 20 μm) of the film. An electrochemical workstation (EG&G Princeton Applied Research) was exploited for cyclic voltammetry measurements with a three-electrode system (KIPIG as a working electrode, Ag/AgCl as a reference electrode, and Pt wire as a counter electrode). The used electrolyte is acetonitrile solution of 10 mM LiI, 1 mM I_2, and 0.1 M $LiClO_4$.

2.2.2. Preparation of Photo Electrodes. The photoelectrodes were prepared according to the procedures described in our previous work.[46] FTO glass plate was pretreated in the aqueous solution of 0.4 mM $TiCl_4$ at 70 °C for 30 min. A commercial TiO_2 sol was doctor-bladed onto the surface of the pretreated FTO, followed by heat-treatment at 325, 373, 450, and 500 °C for 5, 5, 15, and 15 min, respectively. Then, the 0.4 mM $TiCl_4$ solution was used for the

DOI: 10.1021/acs.iecr.9b00795
Ind. Eng. Chem. Res. 2019, 58, 8743−8749

Table 1. Composition (From EDS, Elemental Analysis, and ICP) and Electrochemical Characteristics of Graphene Sheets

	elemental analysis		EDS						
samples	C%	O%	C%	O%	K%	ICP (K) (wt %)	R_s (Ω)	R_{ct} (Ω)	Z_N (Ω)
KIPIG-500	87.88	12.12	95.43	4.35	0.22	0.23	17	10	65
KIPIG-550	86.16	10.84	96.12	3.65	0.23	0.21	16	5	50
KIPIG-600	90.40	9.60	97.21	2.57	0.22	0.27	16	8	57

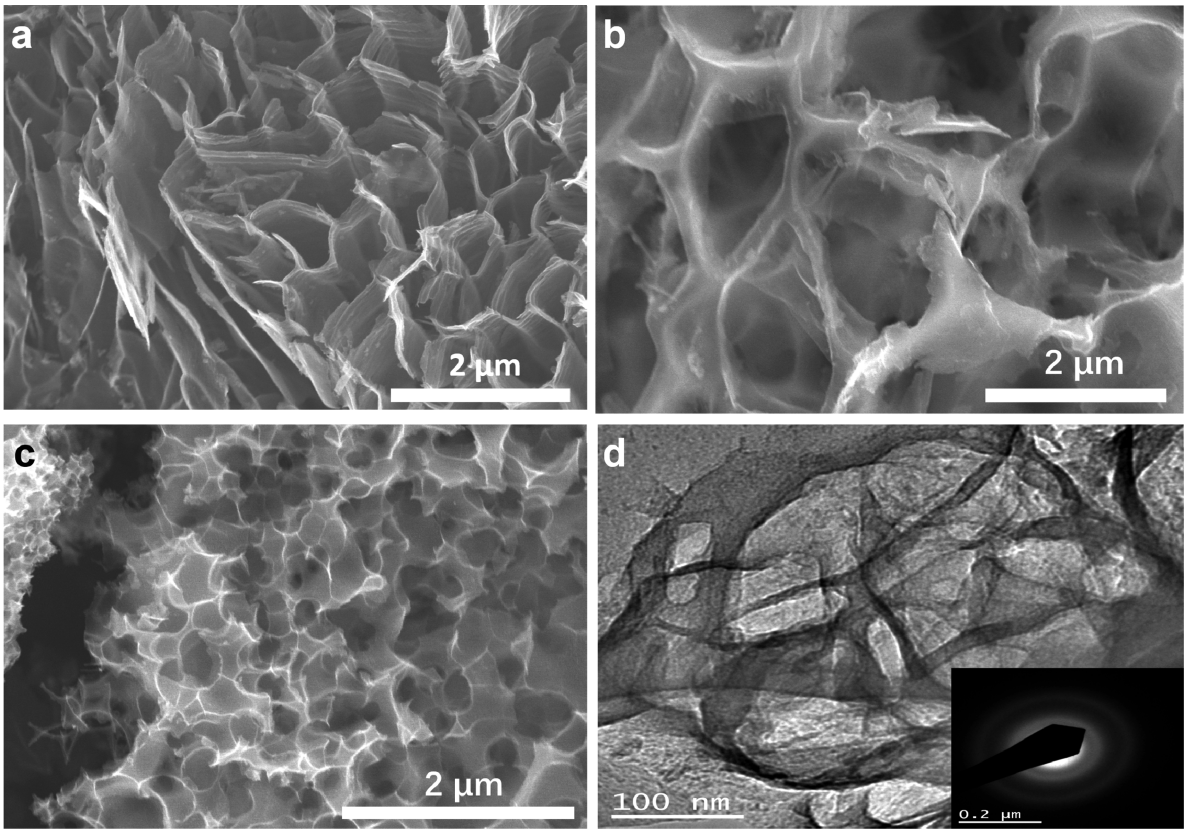

Figure 2. SEM images of (a) KIPIG-500, (b) KIPIG-550, and (c) KIPIG-600. (d) TEM image of KIPIG-550.

post-treatment of the obtained TiO_2/FTO glass plate at 70 °C, followed by heat treatment at 500 °C for 30 min. Lastly, the dye sensitization was completed by immersing the TiO_2 film in a cis-bis(isothiocyanato) bis(2,2′-bipyridyl-4,4′-dicarboxylato)-ruthenium(II)-bis-tetrabutylammonium (N719, 0.3 mM in ethanol) dye solution for 24 h.

2.2.3. Fabrication and Performance Evaluation of DSSCs. A DSSC with of 0.25 cm^2 effective cell area was fabricated by assembling a TiO_2 photoelectrode and a counter electrode with I^-/I_3^- electrolyte.[16] The electrolyte is the solution of 0.025 M LiI, 0.04 M I_2, 0.6 M 1-butyl-3-methylimidazolium iodide (BMII), 0.28 M *tert*-butylpyridine (TBP), and 0.05 M guanidinium thiocyanate in acetonitrile/valeronitrile solvent with 85/15 volume ratio. A solar simulator (Newport) was used to generate 1.5 G sun light illumination (100 mW cm^{-2}) for measurement of the cell performance with Kithley 2400 instrument. CHI 660D electrochemical workstation was exploited for electrochemical impedance spectroscopy (EIS) of DSSCs at open circuit voltage and 10 mV amplitude over the frequency range of 0.1−100 kHz.

2.3. Preparation and Characterization of PSCs. *2.3.1. Synthesis of CH_3NH_3I.* Thirty mL of methylamine (40% in methanol, TCI) was added into 32.3 mL of hydroiodic acid (57 wt % in water, Aldrich) at 0 °C to prepare CH_3NH_3I.[46] The solution was in a rotary evaporator to remove the solvent at 50 °C. Diethyl ether was used to wash the yellowish raw product three times. The recrystallized CH_3NH_3I was collected by filtration and dried in a vacuum oven at 60 °C for 24 h.

2.3.2. Fabrication and Characterization of Perovskite Solar Cells. Perovskite solar cells were fabricated with the method described in our previous work.[46] A compact TiO_2 layer (to prevent direct contact between the FTO and the hole-conducting layer) was coated on FTO substrate by spinning a precursor solution of 15 mM titanium diisopropoxide bis (acetylacetonate), followed by annealing at 500 °C for 30 min. 200 mM $TiCl_4$ solution was used for the post-treatment of the film at 70 °C for 60 min, and distilled water and ethanol were employed to wash it, followed by annealing at 500 °C for 30 min in air. The solution (460 mg mL^{-1}) of PbI_2 in *N*,*N*-dimethylformamide was spin-coated on the top of the TiO_2 layer at 3000 rpm for 30 s, gently dried in air, and heated up to 70 °C for 15 min. Then, the solution of CH_3NH_3I in 2-propanol (with KIPIG powder) was spin-coated on the top of the film at 3000 rpm for 20s. As a result, $CH_3NH_3PbI_3$ perovskite was formed on TiO_2 layer. Finally, a perovskite solar cell was fabricated by doctor-blading KIPIG counter electrode on the film. Electrochemical workstation

DOI: 10.1021/acs.iecr.9b00795
Ind. Eng. Chem. Res. 2019, 58, 8743−8749

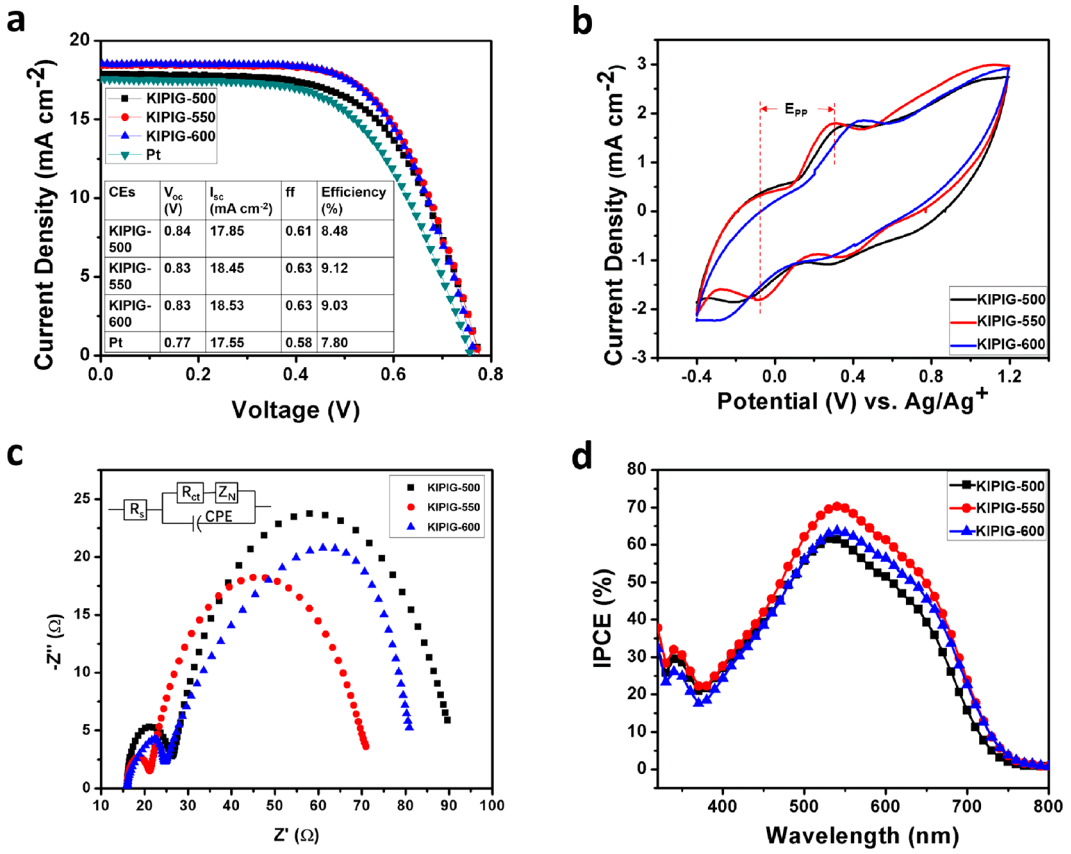

Figure 3. Electrochemical characterization of KIPIG as counter electrode for DSSCs. (a) *I*−*V* curves, (b) CV curves, (c) EIS, inset: the corresponding circuit model, and (d) IPCE curves.

(EG&G Princeton Applied Research) was employed for the cell performance measurements under simulated 1.5 G light irradiation (100 mW cm^{-2}). A monochromator (Newport) was used for incident photon-to-current conversion efficiency (IPCE) curves. CHI 760E electrochemical workstation was exploited for electrochemical impedance spectroscopy (EIS) at open circuit voltage and 10 mV amplitude over the frequency range of 1−100 kHz using under dark condition.

3. RESULTS AND DISCUSSION

As shown in Figure 1a, the invented reaction of K liquid and CO gas was supported by thermodynamic calculations, namely, the thermodynamic feasibility and energy economy of this reaction were confirmed by negative Gibbs free energy change and enthalpy change. The role of simultaneously produced K_2CO_3 is to prevent graphite formation by isolating graphene sheets.

The reaction between K and CO was carried out to synthesize 3D potassium-ion preintercalated graphene (KIPIG) as follows: Potassium was first placed in a ceramic tube reactor. Then the CO gas was introduced into the system at 50 psi at initial. The temperature of the reactor increased from room temperature to the target temperature (500 °C, 550 °C, 600 °C) by 10 °C min^{-1}. XRD measurement was employed to identify the black products. As shown in Figure 1b, K_2CO_3's diffraction peaks can be observed, which confirms the reaction of K and CO. Hydrochloric acid was then used to post-treat the products to remove K_2CO_3. Elemental analysis and EDS identified the obtained black powder is carbon (Table 1). Figure 1c shows the XRD pattern of the black powder obtained after all the treatment. Two broad peaks at 2θ = 26.1° (002) and 43.2° (100) were obtained for all the three samples, indicating the formation of an amorphous phase. Moreover, a larger interlayer space of 3.56 Å was calculated based on XRD result. The obtained carbon nanomaterials were fully investigated by Raman spectroscopy, because it is a useful nondestructive tool to characterize carbonaceous materials, particularly for distinguishing ordered and disordered carbon structures, the in-phase vibration of the graphite lattice (G band, 1575 cm^{-1}) and the disorder band caused by the granite edges (D band, 1355 cm^{-1}). In the Raman spectrum of carbon nanomaterials (Figure 1d), a typical D band and G band were observed for all samples, indicating rich defects in the graphene sheets. Furthermore, inductively coupled plasma (ICP) results show there are about 0.2 wt % K^+ in the materials. The samples were named as KIPIG-500, KIPIG-550, and KIPIG-600 afterward, for those obtained at 500 °C, 550 °C, and 600 °C, respectively.

As shown in Figure 2a−c, the obtained carbon nanomaterials possess a 3D sheets structure. The thickness of the wall of one mesopore is about 2 nm, indicating the layer number of one sheet is about 6. This 3D sheet structure was further evaluated by TEM. The TEM image (KIPIG-550) (Figure 2d) shows the sheet-like structure and the electron diffraction pattern shows poly crystalline ring patterns because of its curved shape. N_2 adsorption was used to measure the surface areas and pore size distributions. The BET surface areas are 1200, 871, and 668 m^2 g^{-1} for KIPIG-500, KIPIG-550, and KIPIG-600, respectively, which indicates that the increasing synthesis temperature led to the decrease in surface area. This

DOI: 10.1021/acs.iecr.9b00795
Ind. Eng. Chem. Res. 2019, 58, 8743−8749

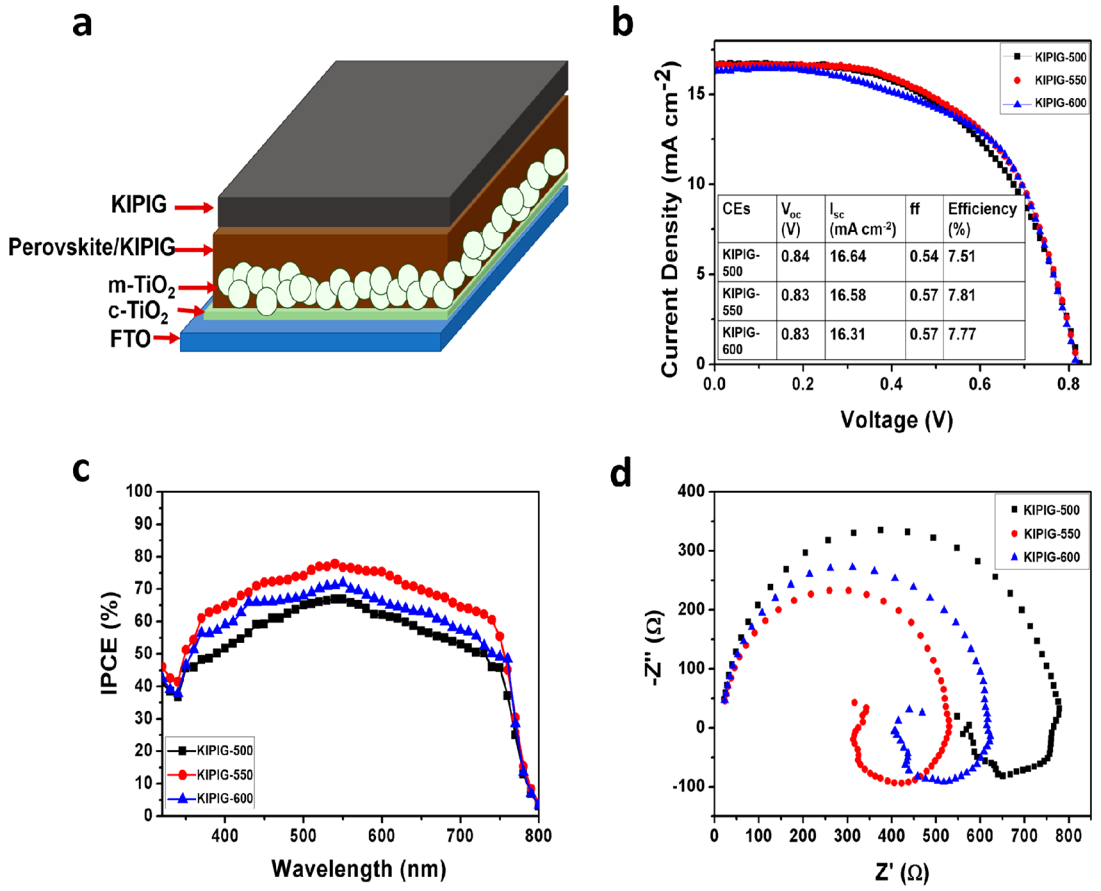

Figure 4. (a) Cell configuration of PSCs. (b) $I-V$ curves, (c) IPCE curves, and (d) EIS of PSCs with KIPIG counter electrodes.

may be because the graphene sheets are easier to stack together and thus lose surface area at higher temperatures. Furthermore, the mesopores and macropores are favorable for liquid diffusion through the pores. A large surface area can provide large electrode/electrolyte interface and thus a large number of active sites. However, the high surface area will lead to low conductivity in normal cases. The electrical conductivity of the 3D graphene was evaluated. The sheet resistance of the carbon film is 10.12 kΩ sq^{-1}, 5.26 kΩ sq^{-1}, and 3.53 kΩ sq^{-1} for KIPIG-500, KIPIG-550, and KIPIG-600, respectively, indicating the conductivity increased with increasing synthesis temperature. The high conductivity and the large surface area of 3D graphene offer unique opportunities for its application related to energy conversion and storage, such as dye-sensitized solar cells and perovskite solar cells.

The performance of 3D potassium-ion preintercalated graphene (KIPIG) as counter electrode material for DSSCs was evaluated. Figure 3a shows the $I-V$ characteristics measured under simulated sunlight with the intensity of 100 mW cm^{-2} at the range 320−100 nm for DSSCs with counter electrodes composed of carbon nanomaterial and Pt on FTO. Their photovoltaic parameters, such as the short-circuit current density (I_{sc}), open-circuit voltage (V_{oc}), fill factor (ff), and power conversion efficiency are summarized in the table insert the Figure 3a. All KIPIG materials show better performance than Pt, since they could provide more active sites for electrolyte reduction. Among all carbon nanomaterials, KIPIG-550 exhibits the best power conversion efficiency of 9.12% with short-circuit current of 18.45 mA cm^{-2}, open-circuit voltage of 0.78 V, and fill factor of 0.63. It is reported that the conductivity and catalytic activity of counter electrode materials determine the performance of a DSSC.[47] The conductivity of KIPIG increased with increasing the temperature from 500 to 550 °C, resulting in the enhancement of DSSC performance. However, further increase of temperature to 600 °C decreased the efficiency of DSSC. This is because the active sites decreased with decreasing surface area.

This was supported by the evaluation of Cyclic voltammograms (CV). The catalytic activity of the counter electrodes were usually obtained from CV measurement. It was conducted using a three-electrode system: KIPIG working electrode, Pt counter electrode, and Ag/Ag^+ reference electrode. An electrolyte composed of 10 mM LiI, 1 mM I_2, and 0.1 M $LiClO_4$, and a scan rate of 20 mV s^{-1}. Figure 3b shows the CV curves for KIPIG-500, KIPIG-550, and KIPIG-600 samples. In these CV curves, the redox peaks correspond to the redox reaction of I^-/I_3^-. The smaller the separation between the cathodic and anodic peak (namely, the peak to peak separation, E_{pp}), the higher the electrochemical rate constant. It is estimated that the peak to peak separation of KIPIG-550 is about 0.3 V, indicating the highest intrinsic catalytic activity of KIPIG-550 Film. KIPIG-550 also shows the highest redox current density for the I_3^-/I^- reaction, since the porous and thick structure of the carbon layer can create a much larger accessible surface area. The strong correlation of DSSC performance and electrocatalytic characteristic was proved by these consistent results with $I-V$ measurements.

It is established that a change of few ohms of interfacial resistance could result in a great impact on DSSC performance. So electrochemical impedance spectra (EIS) were employed to

DOI: 10.1021/acs.iecr.9b00795
Ind. Eng. Chem. Res. 2019, 58, 8743−8749

understand the performance enhancement mechanism of the KIPIG material. In this work, EIS was measured at open-circuit potential in dark condition, as shown in Figure 3c, which displays two well-defined semicircles. Equivalent circuit (insert of figure) was employed to quantitatively analyze EIS results, in which series resistance, charge-transfer resistances at counter electrode/electrolyte interface and at the TiO_2/dye/electrolyte interface are presented by R_s, R_{ct}, and Z_n. The intercept of the first circle on Z_{real} is the Ohmic serial resistance (R_s) caused by electrolyte, electrodes, and other components such as FTO substrate, KIPIG carbon material coating, etc., whereas the small semicircle is attributed to charge transfer at the carbon film/electrolyte (R_{ct}), respectively. The fitted parameters are summarized in the Table 1. All the three counter electrodes show similar R_s, which can be ignored, indicating their good electrical conductivity. KIPIG-550 shows the smallest charge transfer resistance, which means it has the highest charge transfer rate. This confirms that the catalytic activity of the KIPIG-550 electrode is superior to others. This is also consistent with CV measurements, namely, the larger the accessible surface area, the higher the intrinsic catalytic activity. Furthermore, the $I-V$ measurements was further supported by incident photon-to-current conversion efficiency (IPCE) curves (Figure 3d), in which the best conversion efficiency of a DSSC is obtained with the KIPIG-550 counter electrode. It was also found that the I_{sc} obtained from the $I-V$ measurement (16.92 mA cm^{-2}) is higher than that calculated from the IPCE curve. The discrepancy is due to the difference in illumination conditions. A single wavelength was used for measuring photoresponse in the IPCE test, whereas the $I-V$ measurement was carried out under steady illumination of broadband light with a full spectrum.

3D KIPIG was also employed for HTM free perovskite solar cells. The configuration of fabricated perovskite solar cells was shown in Figure 4a. In this configuration, the HTM layer was eliminated and the noble metal electrode was replaced by 3D KIPIG. Figure 4b shows the $I-V$ characteristics of HTM-free PSCs and the corresponding parameters are listed inset. KIPIG-550 exhibited the highest power conversion efficiency of 7.81% with I_{sc} of 16.58 mA cm^{-2}, V_{oc} of 0.83 V, and ff of 0.57, respectively. The incident photon-to-current conversion efficiency was evaluated to further support the excellent performance of PSCs. A strong spectral response in the range 350−750 nm can be seen in IPCE curve (Figure 4c). The integrated currents based on the IPCE curve are quite similar to those obtained from the $I-V$ curves. Figure 4d shows the Nyquist plot of the PSCs with 3D KIPIG CEs in the frequency range of 1 Hz to 1 MHz with 10 mV AC amplitude. The charge exchange process at the perovskite/CE interface leads to the first semicircle in the high frequency region, whereas the TiO_2/perovskite interface results in the one at low frequencies. An additional recombination pathway, namely, the negative capacitance, was also observed in the low frequency region. The lowest charge transfer resistance at the $CH_3NH_3PbI_3$/carbon interface was obtained for KIPIG-550 based PSC, which shows the smallest radius of the semicircle in the high frequency region. This is also consistent with $I-V$ results.

4. CONCLUSION

In summary, 3D KIPIG was synthesized by a novel approach based on the reaction of K liquid and CO gas. Furthermore, the synthesized 3D KIPIG processes high electrical conductivity and high catalytic activity. Its application in dye-sensitized solar cell and perovskite solar cell obtained high power conversion efficiencies of 9.12% and 7.81%. In addition, the 3D mesoporous graphene is promising for applications in other energy devices, such as batteries and fuel cells.

■ ASSOCIATED CONTENT

Supporting Information

The Supporting Information is available free of charge on the ACS Publications website at DOI: 10.1021/acs.iecr.9b00795.

Schematic diagram of the structure of DSSC, photo of carbon paste and carbon counter electrode, adsorption/desorption curves and pore size distribution of carbon nanomaterials, cross-sectional FESEM images of perovskite solar cell (PDF)

■ AUTHOR INFORMATION

Corresponding Author

*E-mail: yunhangh@mtu.edu.

ORCID

Yun Hang Hu: 0000-0002-5358-8667

Notes

The authors declare no competing financial interest.

■ ACKNOWLEDGMENTS

This work was supported by the U.S. National Science Foundation (CMM1-1661699). Y.H.H. also thank Charles and Carroll McArthur for their great support.

■ REFERENCES

(1) Chow, J.; Kopp, R. J.; Portney, P. R. R Energy. *Science* **2003**, *302*, 1528.
(2) O'Regan, B.; Gratzel, M. M A. *Nature* **1991**, *353*, 737.
(3) Grätzel, M. M Solar. *Inorg. Chem.* **2005**, *44*, 6841.
(4) Wang, H.; Wei, W.; Hu, Y. H. H Efficient. *J. Mater. Chem. A* **2013**, *1*, 6622.
(5) Wang, H.; Wei, W.; Hu, Y. H. H NiO. *Top. Catal.* **2014**, *57*, 607.
(6) Wei, W.; Wang, H.; Hu, Y. H. H Unusual. *J. Mater. Chem. A* **2013**, *1*, 14350.
(7) Wei, W.; Wang, H.; Hu, Y. H. H A. *Int. J. Energy Res.* **2014**, *38*, 1099.
(8) Wei, W.; Sun, K.; Hu, Y. H. H An. *J. Mater. Chem. A* **2016**, *4*, 12398.
(9) Yoon, C. H.; Vittal, R.; Lee, J.; Chae, W.-S.; Kim, K.-J. J Enhanced. *Electrochim. Acta* **2008**, *53*, 2890.
(10) Meng, X.; Yu, C.; Song, X.; Iocozzia, J.; Hong, J.; Rager, M.; Jin, H.; Wang, S.; Huang, L.; Qiu, J.; Lin, Z. Z Scrutinizing. *Angew. Chem., Int. Ed.* **2018**, *57*, 4682.
(11) Meng, X.; Yu, C.; Zhang, X.; Huang, L.; Rager, M.; Hong, J.; Qiu, J.; Lin, Z. Z Active. *Nano Energy* **2018**, *54*, 138.
(12) Xin, X.; He, M.; Han, W.; Jung, J.; Lin, Z. Z Low-cost. *Angew. Chem., Int. Ed.* **2011**, *50*, 11739.
(13) Wu, M.; Lin, X.; Hagfeldt, A.; Ma, T. T Low-cost. *Angew. Chem., Int. Ed.* **2011**, *50*, 3520.
(14) Wang, H.; Wei, W.; Hu, Y. H. H NiO. *Top. Catal.* **2014**, *57*, 607.
(15) Wei, W.; Hu, Y. H. H Synthesis. *Int. J. Energy Res.* **2015**, *39*, 842.
(16) Wei, W.; Sun, K.; Hu, Y. H. H Synthesis. *J. Mater. Chem. A* **2014**, *2*, 16842.
(17) Wei, W.; Sun, K.; Hu, Y. H. H Synthesis. *Ind. Eng. Chem. Res.* **2017**, *56*, 1803.
(18) Wei, W.; Sun, K.; Hu, Y. H. H Direct. *J. Mater. Chem. A* **2016**, *4*, 12054.
(19) Gratzel, M. M The. *Nat. Mater.* **2014**, *13*, 838.

DOI: 10.1021/acs.iecr.9b00795
Ind. Eng. Chem. Res. 2019, 58, 8743−8749

(20) Green, M. A.; Ho-Baillie, A.; Snaith, H. J. J The. *Nat. Photonics* **2014**, *8*, 506.
(21) Park, N.-G. G Organometal. *J. Phys. Chem. Lett.* **2013**, *4*, 2423.
(22) Kim, H.-S.; Lee, C.-R.; Im, J.-H.; Lee, K.-B.; Moehl, T.; Marchioro, A.; Moon, S.-J.; Humphry-Baker, R.; Yum, J.-H.; Moser, J. E.; Grätzel, M.; Park, N.-G. G Lead. *Sci. Rep.* **2012**, *2*, 591.
(23) Meng, X.; Cui, X.; Rager, M.; Zhang, S.; Wang, Z.; Yu, J.; Harn, Y. W.; Kang, Z.; Wagner, B. K.; Liu, Y.; Yu, C.; Qiu, J.; Lin, Z. Z Cascade. *Nano Energy* **2018**, *52*, 123.
(24) Etgar, L.; Gao, P.; Xue, Z.; Peng, Q.; Chandiran, A. K.; Liu, B.; Nazeeruddin, M. K.; Grätzel, M. M Mesoscopic. *J. Am. Chem. Soc.* **2012**, *134*, 17396.
(25) Ku, Z.; Rong, Y.; Xu, M.; Liu, T.; Han, H. H Full. *Sci. Rep.* **2013**, *3*, 3132.
(26) Yang, Y.; Ri, K.; Mei, A.; Liu, L.; Hu, M.; Liu, T.; Li, X.; Han, H. H The. *J. Mater. Chem. A* **2015**, *3*, 9103.
(27) Liu, L.; Mei, A.; Liu, T.; Jiang, P.; Sheng, Y.; Zhang, L.; Han, H. H Fully. *J. Am. Chem. Soc.* **2015**, *137*, 1790.
(28) Li, X.; Tschumi, M.; Han, H.; Babkair, S. S.; Alzubaydi, R. A.; Ansari, A. A.; Habib, S. S.; Nazeeruddin, M. K.; Zakeeruddin, S. M.; Grätzel, M. M Outdoor. *Energy Technol.* **2015**, *3*, 551.
(29) Xiao, Y.; Cheng, N.; Kondamareddy, K. K.; Wang, C.; Liu, P.; Guo, S.; Zhao, X.-Z. Z W-doped. *J. Power Sources* **2017**, *342*, 489.
(30) Xiao, Y.; Wang, C.; Kondamareddy, K. K.; Cheng, N.; Liu, P.; Qiu, Y.; Qi, F.; Kong, S.; Liu, W.; Zhao, X.-Z. Z Efficient. *ACS Appl. Energy Mater.* **2018**, *1*, 5453.
(31) Qi, F.; Wang, C.; Cheng, N.; Liu, P.; Xiao, Y.; Li, F.; Sun, X.; Liu, W.; Guo, S.; Zhao, X.-Z. Z Improving. *Electrochim. Acta* **2018**, *282*, 10.
(32) Bai, S.; Cheng, N.; Yu, Z.; Liu, P.; Wang, C.; Zhao, X.-Z. *Electrochim. Acta* **2016**, *190*, 775.
(33) Wei, Z.; Chen, H.; Yan, K.; Zheng, X.; Yang, S. S Hysteresis-free. *J. Mater. Chem. A* **2015**, *3*, 24226.
(34) Zheng, X.; Chen, H.; Li, Q.; Yang, Y.; Wei, Z.; Bai, Y.; Qiu, Y.; Zhou, D.; Wong, K. S.; Yang, S. S Boron. *Nano Lett.* **2017**, *17*, 2496.
(35) Yan, K.; Wei, Z.; Li, J.; Chen, H.; Yi, Y.; Zheng, X.; Long, X.; Wang, Z.; Wang, J.; Xu, J.; Yang, S. S High-performance. *Small* **2015**, *11*, 2269.
(36) Wei, W.; Hu, B.; Jin, F.; Jing, Z.; Li, Y.; Garcia Blanco, A. A.; Stacchiola, D. J.; Hu, Y. H. H Potassium-chemical. *J. Mater. Chem. A* **2017**, *5*, 7749.
(37) Haddon, R. C.; Hebard, A. F.; Rosseinsky, M. J.; Murphy, D. W.; Duclos, S. J.; Lyons, K. B.; Miller, B.; Rosamilia, J. M.; Fleming, R. M.; Kortan, A. R.; Glarum, S. H.; Makhija, A. V.; Muller, A. J.; Eick, R. H.; Zahurak, S. M.; Tycko, R.; Dabbagh, G.; Thiel, F. A. A Conducting. *Nature* **1991**, *350*, 320.
(38) Hebard, A. F.; Rosseinsky, M. J.; Haddon, R. C.; Murphy, D. W.; Glarum, S. H.; Palstra, T. T. M.; Ramirez, A. P.; Kortan, A. R. R Superconductivity. *Nature* **1991**, *350*, 600.
(39) Chen, J.-H.; Li, L.; Cullen, W. G.; Williams, E. D.; Fuhrer, M. S. S Tunable. *Nat. Phys.* **2011**, *7*, 535.
(40) Ohta, T.; Bostwick, A.; Seyller, T.; Horn, K.; Rotenberg, E. E Controlling. *Science* **2006**, *313*, 951.
(41) Pan, J.-W.; Bouwmeester, D.; Weinfurter, H.; Zeilinger, A. A Experimental. *Phys. Rev. Lett.* **1998**, *80*, 3891.
(42) Wei, W.; Chang, L.; Sun, K.; Pak, A. J.; Paek, E.; Hwang, G. S.; Hu, Y. H. H The. *Nano Lett.* **2016**, *16*, 8029.
(43) Wei, W.; Hu, Y. H. H Highly. *J. Mater. Chem. A* **2017**, *5*, 24126.
(44) Chang, L.; Wei, W.; Sun, K.; Hu, Y. H. H Excellent. *J. Mater. Chem. A* **2017**, *5*, 9090.
(45) Chang, L.; Stacchiola, D. J.; Hu, Y. H. H Design. *Ind. Eng. Chem. Res.* **2018**, *57*, 3610.
(46) Wei, W.; Stacchiola, D.; Akter, N.; Boscoboinik, J. A.; Hu, Y. H. H Lithium-chemical. *ACS Appl. Energy Mater.* **2019**, *2*, 1445.
(47) Kavan, L.; Yum, J.-H.; Nazeeruddin, M. K.; Grätzel, M. M Graphene. *ACS Nano* **2011**, *5*, 9171.

DOI: 10.1021/acs.iecr.9b00795
Ind. Eng. Chem. Res. 2019, 58, 8743−8749